PCCP

ROYAL SOCIETY OF CHEMISTRY

PAPER

View Article Online
View Journal | View Issue

Check for updates

Cite this: *Phys. Chem. Chem. Phys.*, 2020, **22**, 25819

Ultrafast carrier relaxation dynamics of photoexcited GaAs and GaAs/AlGaAs nanowire array†

Bowen Zhang,[ab] Zhaogang Nie,*[b] Bo Wang,[b] Dengkui Wang,[a] Jilong Tang,[a] Xiaohua Wang,*[a] Jiahua Zhang,[c] Guichuan Xing,[d] Wenchun Zhang[e] and Zhipeng Wei*[a]

Received 11th August 2020,
Accepted 19th October 2020

DOI: 10.1039/d0cp04250a

rsc.li/pccp

Femtosecond optical pump–probe spectroscopy is employed to elucidate the ultrafast carrier nonradiative relaxation dynamics of bare GaAs and a core–shell GaAs/AlGaAs semiconductor nanowire array. Different from the single nanowire conventionally used for the study of ultrafast dynamics, a simple spin coating and peeling off method was performed to prepare transparent organic films containing a vertical oriented nanowire array for transient absorption measurement. The transient experiment provides the direct observation of carrier thermalization, carrier cooling, thermal dissipation and band-gap energy evolutions along with the carrier relaxations. Carrier thermalization occurs within sub-0.5 ps and proceeds almost independently on the AlGaAs-coating, while the time constants of carrier cooling and thermal dissipation are increased by an order of magnitude due to the AlGaAs-coating effect. The concomitant band-gap evolutions in GaAs and GaAs/AlGaAs include an initial rapid red-shift in thermalization period, followed by a slow blue and/or red shift in carrier cooling, and then by an even slower blue shift in thermal dissipation. The evolution is explained by the competition of band-gap renormalization, plasma screening and band-filling. These findings are significant for understanding the basic physics of carrier scattering, and also for the development of flexible optoelectronic devices.

Introduction

Due to their unique physical properties, such as direct band-gap, high electron mobility and ultrashort charge carrier lifetimes, III–V bare GaAs and core–shell GaAs/AlGaAs semiconductor nanowires (SNWs) have been considered as excellent building blocks for electronic and optoelectronic devices,[1–3] and thus have attracted much attention over the past few decades.[4–11] It has been reported that the AlGaAs-shell in GaAs/AlGaAs heterostructure SNWs can effectively passivate the high-density surface states of the GaAs-core, leading to improvement of radiative efficiency and photoresponsivity in GaAs-based optoelectronic devices.[7,12,13] Most of the on-going research studies are aimed at exploring the vast possibilities of novel device design based on SNWs.[5–7,11,14–17] These applications necessitate a detailed understanding of their fundamental carrier dynamics, since the device performance is ultimately limited by the microscopic carrier relaxation or scattering process.[18–21] The study of ultrafast carrier relaxation dynamics in GaAs and GaAs/AlGaAs SNWs is consequently significant not only for understanding of the basic physics of carrier scattering, but also for the development of high-speed electronic and optoelectronic devices.

Photoexcited carrier phenomena in semiconductors have been extensively studied for decades with a variety of experimental approaches.[16,18,22–24] Recent advances in femtosecond laser generation and time-resolved spectroscopic techniques have made it possible to achieve direct observation of transient processes on a femtosecond time scale.[19–21,25] Nevertheless, despite a number of studies addressing the ultrafast carrier dynamics in bulk GaAs and AlGaAs and their 2D quantum well materials,[22,23,26,27] there have been very few transient experiments performed on their 1D nanostructures.[24,28] Several previous studies utilized time-resolved photoluminescence (PL) and time-resolved

[a] *State Key Laboratory of High-Power Semiconductor Laser, School of Science, Changchun University of Science and Technology, 7089 Wei-Xing Road, Changchun 130022, China. E-mail: zpweicust@126.com*
[b] *School of Physics and Optoelectronic Engineering, Guangdong University of Technology, Guangzhou 510006, China. E-mail: zgnie@gdut.edu.cn*
[c] *State Key Laboratory of Luminescence and Applications, Changchun Institute of Optics, Fine Mechanics and Physics, Chinese Academy of Sciences, 3888 Eastern South Lake Road, Changchun 130033, China*
[d] *Institute of Applied Physics and Materials Engineering, University of Macau, Macao SAR 999078, China*
[e] *College of Traditional Chinese Medicine, Jiangxi University of Traditional Chinese Medicine, Nanchang 330004, China*

† Electronic supplementary information (ESI) available. See DOI: 10.1039/d0cp04250a

photocurrent experiments to investigate the response speed and response intensity of GaAs and GaAs/AlGaAs SNWs.[16,24,29–31] Firstly, these experiments did not pay much attention to the ultrafast carrier nonradiative relaxation process, such as hot carrier thermalization and cooling, which occurs immediately after photoexcitation and play a crucial role for subsequent long-lived dynamics. Secondly, these studies were mostly focused on single SNWs.[24,28,32] In these experiments, the single SNW structures are typically much smaller than the laser focus size, and thus the probed transient signal is usually overwhelmed by the background light scattering.[24,25,33–35] Moreover, the focusing lens system used in these transient and PL experiments greatly limits the improvement of the time-resolution (typically in hundreds of femtoseconds and even in picoseconds).[24,30] In contrast to individual SNWs, an ultrafast optical study of ordered SNW-array with large-area controllable spacing, orientation and size is also quite important, since a variety of practical technological applications necessitate the implementation of SNW-array,[36–39] especially for the applications where vertical oriented SNWs are required to allow electrical contact to many nanowires in parallel, for example, in edge emitting lasers[40] and array solar cells.[41–44] However, studies on their carrier dynamics *via* ultrafast optical experiments were usually hampered by the optical properties of SNW-array, such as the opaque substrate used in SNW growth and the poor reflection of the sample surface, which severely degrade the S/N ratio of the probed signals. To date, despite a few studies dedicated to the excitonic dynamics in single SNWs, a detailed investigation of carrier nonradiative relaxation in GaAs and GaAs/AlGaAs SNW-array remains unexplored experimentally.

In this study, a simple spin coating and peeling off method is used to prepare a transparent and flexible organic film, which contains upright GaAs and GaAs/AlGaAs SNW arrays. The laser beam can penetrate the film without serious light scattering and reflections, making it quite suitable for ultrafast transient absorption measurement. With this strategy, our experiments provide the first observation, as far as we know, of a series of ultrafast carrier relaxation dynamics, such as carrier thermalization, carrier cooling and thermal dissipation. The time constants and their dependence on AlGaAs-coating and pump wavelengths are discussed. In addition, the evolution of band-gap energy of GaAs along with the carrier relaxation process is also discussed in chronological order.

Experimental

Sample fabrication and optical characterizations

The GaAs and GaAs/AlGaAs SNW arrays were both grown by a Ga-assisted self-catalyzed method on Si(111) substrates with a DCA P600 solid source MBE system.[45,46] For the GaAs/AlGaAs core–shell SNWs, the growth processes of the GaAs core are the same as those of the bare GaAs SNWs. After the GaAs-core growth was finished, the beam equivalent pressure (BEP) of Ga and As was kept unchanged and turned on the Al flux with a specific BEP for several minutes for the growth of the AlGaAs-shell.

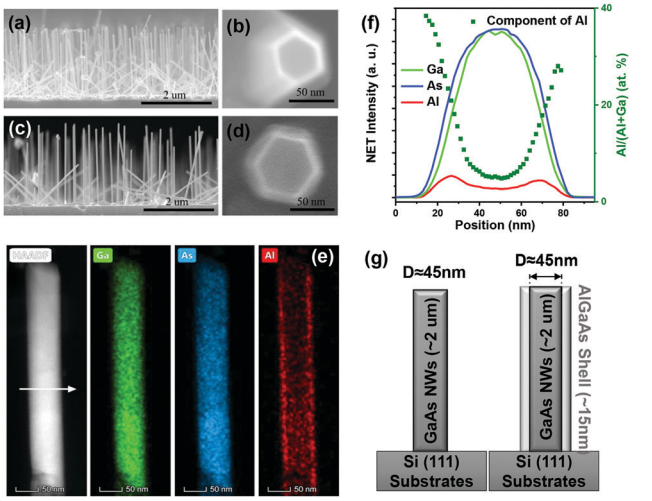

Fig. 1 (a and b) SEM images of GaAs SNWs revealing an average diameter of 45 nm and an average length of 2 μm. (c and d) SEM images of GaAs/AlGaAs SNWs indicating an average diameter of 75 nm and an average length of 2 μm. (e) HAADF-STEM image and EDS elemental maps of the cross-section of a single GaAs/AlGaAs SNW. (f) EDX spectra of the cross section, illustrating the net intensity distribution of the metal elements. (g) Schematic of bare GaAs and core–shell GaAs SNW structure grown on the Si(111) substrate.

The detailed fabrication procedure is described in Section S1 of the ESI.† The SEM images (see Fig. 1a–d) were obtained using a field emission scanning electron microscope (SEM, Hitach, SU8220). The high-angle annular dark field scanning transmission electron microscopy (HAADF-STEM) with energy-dispersive X-Ray spectroscopy (EDX) of the SNWs (see Fig. 1e) and high-resolution transmission electron microscopy (HRTEM) (see Fig. S1a–c, ESI†) were obtained using a Talos F200S electron microscope operated at an accelerating voltage of 200 kV. X-ray diffraction (XRD) (Bruker, D8 Focus) using Cu Ka radiation was utilized to confirm the crystal structure of nanowires (see Fig. S1d, ESI†). The temperature dependent photoluminescence (PL) was recorded using a HORIBA iHR 550 detector with a 655 nm semiconductor diode laser as the excitation source (see Fig. S1e, f and S4, ESI†).

Transparent film sample preparation for ultrafast spectra characterization

As mentioned above, the Si substrate used in MBE is not transparent and the scattered light from the array surface is conventionally too diffuse to be collected for signal detection. Here, inspired by an early strategy,[2,3] we prepared transparent and flexible organic films, which contain an upright SNW array, with a simple spin coating and peeling off method. As illustrated in Fig. 2a, the procedure is as follows: (i) PDMS (polydimethylsiloxane, Dow Corning SYLGARD 184) is firstly dropped on the sample surface. (ii) The sample is kept under vacuum for 15 minutes to remove internal bubbles. (iii) It is placed in a spin coating machine to ensure the uniformity of the film, followed by heating at 80 °C for two hours for curing. The spin coating and curing processes are both carried out in a nitrogen atmosphere. Finally, (iv) the

transparent PDMS film with free standing SNWs, subsequently used in the transient absorption measurement, is carefully peeled off with tweezers.

Ultrafast spectra characterization

Optical pump–probe measurements are performed with narrowband pump pulses and broadband probe pulses. A detailed description of the setup was presented in our previous work.[47,48] The broadband pulses (~480–950 nm) with a sub-10 fs duration are produced by spectral broadening of the 35 fs output from an amplified Ti:sapphire laser source (800 nm center wavelength, 35 fs pulse width and 1 kHz repeation rate) in a noble gas filled hollow-core-fiber followed by chirped mirror compression. The narrowband 800 nm pump beam is from a part of the beam separated from the amplified Ti:sapphire laser source, while the narrowband 650 nm pump laser was generated by inserting bandpass filters with a 20 nm width into the broadband pump pulse. The probe pulse is from a small part of the broadband pulse separated from the sub-10 fs pulse. The pump and probe beams are orthogonally polarized to minimize the coherent artifacts in the measured signal, which can be further suppressed by singular-value decomposition of the 2D probe energy–time delay data set. The transient absorption signal was obtained by measuring the normalized differential absorbance spectra $\Delta A = -\log_{10}(1 + \Delta T/T)$, where $\Delta T/T = (T_{on} - T_{off})/T_{off}$, T_{on} and T_{off} are the intensity of the transmitted probe light passing through the sample in both the presence and absence of the pump excitation. The time resolution of the experimental apparatus was determined by the second-order intensity cross-correlation between pump and probe pulses, which yields a resolution of ~55–60 fs for a Gaussian pulse (see Fig. S2, ESI†). The spot size of pump and probe on the sample are 220 μm (113 μJ cm^{-2}) and 130 μm (58 μJ cm^{-2}) for the 800 nm experiment, and 440 μm (49 μJ cm^{-2}) and 200 μm (33 μJ cm^{-2}) for the 650 nm experiment. All measurements are performed at room-temperature (RT, 300 K). Excitation pump fluence-dependence measurements were performed to verify that photoexcitation of the sample occurs in the one-photon regime (see Fig. S3, ESI†).

Results and discussion

The SEM images of bare GaAs and GaAs/AlGaAs SNW arrays are shown in Fig. 1a and c, respectively. The average lengths of these SNWs is about 2 μm, much longer than their average diameters, as displayed by the SEM end-images of single GaAs and GaAs/AlGaAs SNWs in Fig. 1b and d, which reveals a hexagonal shape with average diameters of ~45 nm and ~75 nm, respectively. In order to figure out more information regarding the interface characteristics in GaAs/AlGaAs SNWs, STEM investigations were performed on individual SNW. The HAADF-STEM images and the corresponding EDS elemental maps of the cross-section from different angles are presented in Fig. 1e for GaAs/AlGaAs SNWs. From the distribution of Al components in the EDX spectra in Fig. 1f, the AlGaAs shell thickness is around 15 nm. The average diameter of the inner GaAs-core is also ~45 nm, approximately equal to the size of bare GaAs SNWs. It is noted that there isn't a sharp step-like

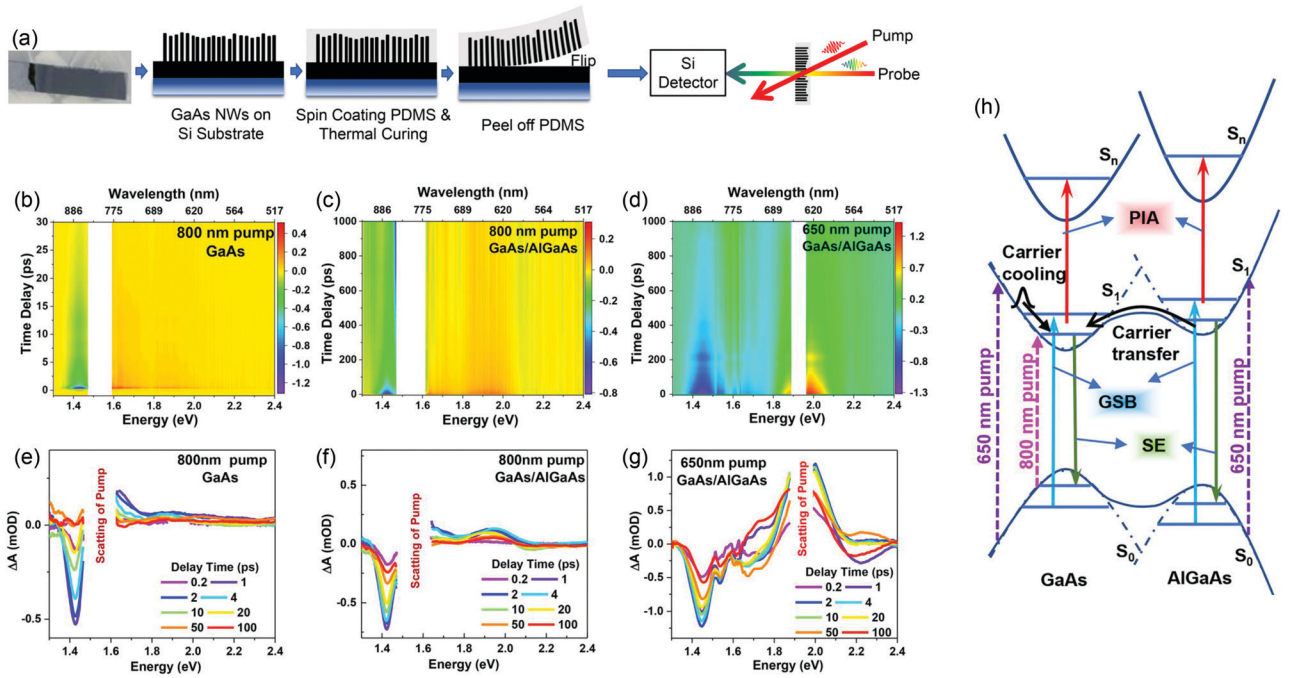

Fig. 2 (a) Schematic illustration of the procedure used to prepare the SNW-array film for ΔA measurement. (b–d) The ΔA spectra of GaAs and GaAs/AlGaAs SNW-array using a 500–950 nm probe pulse under 650 nm and 800 nm pumps. The scattering from the pump (650 nm or 800 nm) was removed for clarity. (e–g) ΔA spectra at several delay times for GaAs and GaAs/AlGaAs SNW-arrays. (h) Schematic of the bandgap structures of GaAs and GaAs/AlGaAs, and the photoexcited transitions in the ΔA spectra.

change from GaAs-core to AlGaAs-shell, thus it is reasonable to confirm the existence of a thin gradient layer between core and shell materials. Based on the sizes obtained, a schematic of GaAs and core–shell AlGaAs structures on Si(111) substrates is illustrated in Fig. 1g.

Fig. 2a demonstrates the PDMS stripping method used to peel off the SNW array for ΔA measurement. The solidified PDMS is transparent in our pump and probe wavelength range. In contrast to the situation in which the SNWs are in air, to immerse the SNWs in PDMS surrounding with a refractive index ($\sim$1.43) larger than that of the air ($\sim$1) could be a reason to reduce the laser scattering when the beam passes through the sample film. The prepared organic film can be further transferred to a plastic substrate, thus it is meaningful for the development of flexible GaAs and GaAs/AlGaAs SNW-array-based devices.[2,3]

As shown in Fig. 2b–d, the temporal evolution of the differential absorption (ΔA) spectra as a function of pump–probe time delay were obtained by the selective excitation of GaAs and GaAs/AlGaAs SNW-arrays with 800 nm (1.55 eV) and 650 nm (1.91 eV) pulses, respectively. The scattering wavelength ranges from pump pulses were removed for clarity. For comparison purposes, the ΔA spectra at several delay times from 0.5 ps to 100 ps were displayed in Fig. 2e–g. Firstly, for all the ΔA profiles, there are obvious grand-state bleaching (GSB) signals peaking at $\sim$1.43 eV (867 nm), quite close to the bandgap edge of GaAs with a zinc blende (ZB) crystal phase ($\sim$1.426 eV).[49] The schematic of the bandgap structures and the photoexcited transitions in GaAs and GaAs/AlGaAs are shown in Fig. 2h. Carrier-induced broadening and phase-space filling can both be responsible for the exciton absorption bleaching,[18,50] which will be discussed further later. Note that there are actually two crystal phases, wurtzite (WZ) and zinc blende (ZB), in the GaAs SNWs,[51,52] as distinguished in Fig. S1b (ESI†), where they pile up layer by layer to form the GaAs SNWs. PL measurement indicates that the bandgap of GaAs with WZ phase is only 20 meV larger than that of ZB GaAs at RT (see Fig. S4, ESI†).[51,52] Thus, the broad GSB at $\sim$1.43 eV may contain the contributions from these two phases. However, to quantitatively determine the exact energy difference is still under debate,[53–56] and in our experiments we didn't obtain a distinguishable dynamics difference between them. In addition, a careful inspection of the GSB peak position at 1.428 eV under 800 nm pumps suggests a slight red shift in comparison with that at 1.452 eV upon 650 nm pumps. It could be resulted from the spectral overlap between the 800 nm-pump scattering and partial GSB bands on the high-energy side, which consequently shifts the GSB to the red side.

Except for the GSB bands, a salient positive photoinduced absorption (PIA) band at 1.554 eV and a weak one at 1.908 eV were also observed under 800 nm pump for bare GaAs and core–shell GaAs/AlGaAs. They can be attributed to carrier-induced broadening of the excitonic transitions or excited-state absorption (ESP) involving inter-subband transitions,[18] as illustrated in Fig. 2(h). It can be seen that the strong PIA band at 1.554 eV is obviously cut down and shifts to the blue side while the weak one at 1.908 eV is greatly enhanced when the pump wavelength is changed from 800 nm to 650 nm. The variation of the PIAs upon higher energy pump is probably due to the overlaps among the ΔA signals of the core, shell and its gradient layer. It has been reported that the doping of Al element in the $Al_xGa_{1-x}As$ gradient layer will increase the band-gap, and the band-gap of AlGaAs is $\sim$2.0 eV,[49] quite close to the PIA at 1.908 eV. With the 650 nm pump, all the GaAs, AlGaAs and even $Al_xGa_{1-x}As$ can be excited. However, the decomposition of the spectral features in terms of the various ultrafast processes requires further experimental and theoretical investigations, that are beyond the scope of this study. In our analysis, we will concentrate on the dynamics of the GSB at $\sim$1.43 eV due to band edge transitions of GaAs, which plays dominant roles currently in most practical applications.[5,7,36,37,43]

The GSB dynamics due to the band-gap excitonic transition ($\sim$1.43 eV) for GaAs and GaAs/AlGaAs SNW-arrays are shown in Fig. 3. All the signals are negative and can be accurately reproduced by three exponential components. The instrument response function, which dictates the time-resolution ($\sim$55–60 fs for a Gaussian pulse, see Fig. S2, ESI†) of the experimental apparatus, has been convoluted with the exponential decay function in order to extract accurate time constants for the decay components. The zero delay is defined as the coincidence of the pump and probe maxima. Since the pump and probe energies are different, an additional advantage of the experiment is that the coherence effects at the zero-time position can in principle be avoided.[23] The fitting results are presented in Table 1. For the signals obtained with 800 nm pumps, the exponential decay

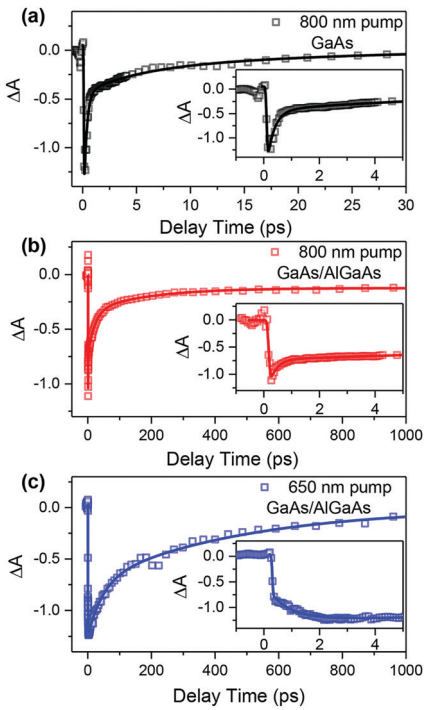

Fig. 3 GSB dynamics of GaAs (a) and GaAs/AlGaAs (b) SNW-array probed at 1.423 eV under an 800 nm pump. (c) GSB dynamics of the GaAs/AlGaAs SNW-array probed at 1.447 eV under the 650 nm pump.

Table 1 Exponential fitting results of GSB signals of GaAs and GaAs/AlGaAs SNW-arrays with 800 nm and 650 nm pumps

Sample	Pump (nm)	τ_1 (ps)	τ_2 (ps)	τ_3 (ps)
GaAs	800	0.26 ± 0.02	5 ± 2	25 ± 10
GaAs/AlGaAs	800	0.27 ± 0.04	22 ± 4	190 ± 60
GaAs/AlGaAs	650	0.77 ± 0.04	47 ± 4	475 ± 25

exhibits an initial rapid decay (τ_1) of the photo-bleaching followed by two slower recoveries (τ_2 and τ_3), similar to those reported previously for semiconductor GaAs quantum wells.[23,26] For the sake of clarity, partial traces close to the zero-time position are enlarged in the insets of Fig. 3 to show the initial rapid dynamics. As listed in Table 1, the initial part appears to be an ultrafast sub-0.5 ps decay component, which is hitherto unobserved due to the limited time resolution employed in previous time-resolved studies of GaAs SNWs, although a measurement of GaAs quantum wells suggests a carrier thermalization time of several hundred femtoseconds.[23,57] For the traces obtained by the 650 nm pump ($\sim$350 meV higher than the 800 nm pump) for the GaAs/AlGaAs SNW-array, the initial decay processes disappear and are replaced by an ultrafast rise process, which is probably due to the ultrafast carrier transfer from the AlGaAs-shell to GaAs-core. The following dynamics is quite similar to those under 800 nm excitation, except that the time constants are increased appreciably.

In principle, an initial nonequilibrium electron–hole distribution with a relatively localized density in momentum space is generated immediately following the incidence of femtosecond laser pulse. After that, a hot quasi-equilibrium Fermi–Dirac distribution is typically realized on a typical time scale of several hundred femtoseconds up to a few picoseconds in semiconductor materials.[18,50] In this period, the electrons and holes randomize their momenta through carrier–carrier and carrier–(typically LO) phonon scatterings, leading to the formation of hot excitons with a carrier temperature much higher than that of the lattice.[18,47] It has been proved recently that the injected free charge carriers are about twice more efficient on inducing transient absorption than excitons.[58] According to the analysis above, the τ_1 could be assigned to the initial carrier thermalization process. As shown in Table 1, there isn't an obvious τ_1 change from GaAs to GaAs/AlGaAs under 800 nm pumps, indicative of insensitive dependence on the AlGaAs-coating effect. As τ_1 is extremely short, it is probably because the carriers have not had enough time to spread to the surface trap states, so that the coating effect has yet to come into play. Indeed, extremely fast carrier–carrier scattering is the dominant thermalization mechanism, while for electron–phonon scattering, which takes part in the surface states trapping process, it is not fast enough to explain the rapid thermalization. In addition, since the penetration depth ($\sim$0.3–0.7 μm)[59] of the light used here is much larger than the thickness of the AlGaAs shell, it is inevitable that the shell and core of GaAs/AlGaAs are both excited by a 650 nm pump laser. As such, it is possible that the initial rapid decay due to the GaAs core itself is buried by the stronger rise process. The possiblility of the rapid decay in GaAs/AlGaAs under the 650 nm pump will be further discussed in terms of the time-dependent band-gap.

After the rapid thermalization, the hot excitons formed continue to cool down and relax to the bottom of the conduction (or valence) bands through carrier–phonon scattering and at later times *via* even slower acoustic phonon emissions. For bare GaAs, the fast carrier cooling (or heating of the lattice) dynamics has a characteristic time of a few picoseconds (τ_2, $\sim$5 ps), while the slower thermal dissipation to the ambient matrix (such as PDMS) takes a time constant (τ_3) of tens and even hundreds of picoseconds. The time scale of τ_2 is comparable to the characteristic time of carrier transport in quasi-1D GaAs SNWs, verified recently by transient Rayleigh scattering measurement.[24] The most striking result in Table 1 is that the time constants, τ_2 and τ_3, of GaAs/AlGaAs are an order of magnitude longer than those of the bare GaAs SNWAs, whether under 800 nm or 650 nm excitations. The τ_2 increases from several picoseconds to tens of picoseconds, while τ_3 is from tens to several hundreds of picoseconds. This is evidence that the AlGaAs-shell can significantly prolong the carrier cooling times, probably arising from the effective passivation of the high-density surface states. In addition, in the period of thermal dissipation, the energy consumption can also be achieved by radiative and non-radiative recombination, such as an Auger-type process which is also a phonon-assisted process. It also occurs typically on a time scale of tens or even hundreds of picoseconds,[60,61] and thus it not expected to contribute significantly to the decays with time constants of several hundreds of femtoseconds.

Along with the nonradiative carrier relaxation process, the band-gap energy (E_g) of the semiconductors can be modulated by various nonlinear effects, such as band-gap renormalization (BGR) and band-filling (BF, or dynamic Burstein–Moss effect).[23,26,27,57,62] These effects compete with each other, resulting in time-dependent E_g, which serves as a delicate probe of the interactions between nonequilibrium carriers as a function of time delay, and can be discerned from the temporal evolution of spectral first moment ($M_1(t)$),[47,63] defined as

$$M_1(t) = \int_{E_i}^{E_f} E\Delta A(E)\mathrm{d}E \Big/ \int_{E_i}^{E_f} \Delta A(E)\mathrm{d}E \qquad (1)$$

where, t is the pump–probe time delay, E is the probe photon energy (in eV), E_i and E_f correspond to the limits of the integral, respectively, and $\Delta A(E)$ is the ΔA spectra as a function of the probe photon energy. The $M_1(t)$ gives the valence–conduction energy gap weighted by the carrier distribution functions,[6,47] which is intuitively related to the evolution of E_g between the bands which are optically coupled by the probe pulse.

The calculated $M_1(t)$ traces for the GSBs with different pumps are shown in Fig. 4. Based on the carrier relaxation dynamics addressed above, the evolution of E_g can be adequately described by three stages in chronological order. The $M_1(t)$ traces in the initial time range close to time zero (Stage I) are compared with the evolution of FWHM (green lines) of GSB bands in (a–c). In

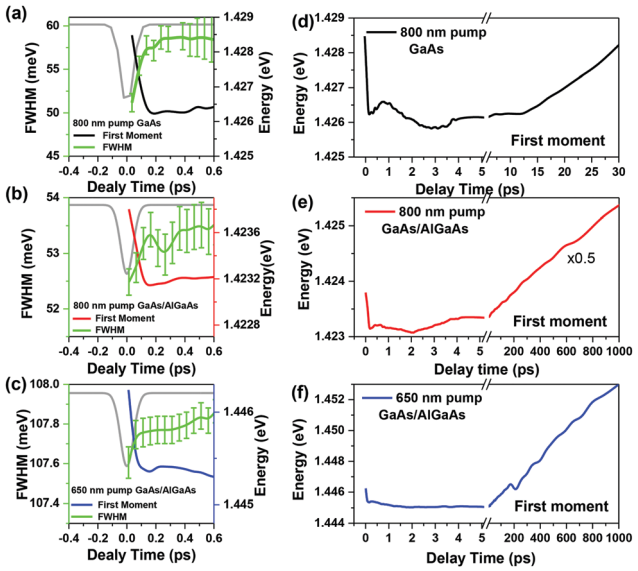

Fig. 4 $M_1(t)$ traces of GSB dynamics due to the bandgap transition in GaAs and GaAs/AlGaAs SNW-arrays under 800 nm and 650 nm pumps. The $M_1(t)$ traces in the initial time range before 0.6 ps are compared with the evolution of FWHM (green lines) of GSB bands in (a–c). The instrument response profiles (gray lines) without vertical coordinates are used to indicate the zero-time positions. The $M_1(t)$ traces in longer time ranges corresponding to carrier cooling are shown in (d–f).

Stage I within the initial thermalization time range, an extremely fast red-shift (~1–2 meV) happens within 0.2 ps for GaAs and GaAs/AlGaAs SNW-arrays immediately after the laser excitation. The time is in the range of τ_1 without AlGaAs-coating, and is several times that of the time resolution (~55–60 fs). We rule out the possibility that the signal is due to interference close to the time zero position because the pump and probe are at different wavelengths. The red-shift, which happens when the pumped hot carriers exist in the form of electron–hole plasma (or hot quasi-exciton), arises from plasma-induced BGR and screening of the exciton binding energy.[18]

The excitonic resonance abruptly shifts to red as hot carriers are injected into the bands by incident pumps with energies (more than 100 meV, this experiment) in excess of the band gap, and due to the strong collisions among free carriers or excitons, the shift occurs simultaneously with the increase in width (full width at half-maximum, FWHM) of the GSB bands,[64,65] as shown in Fig. 4a–c, and the decrease in the peak absorbance, which is the origin of the bleaching at the initial time range.[23,50] The observed energy shift is an order of magnitude larger than those reported in conventional 2D semiconductors such as GaAs quantum wells (~0.1 meV),[66] probably as a consequence of the much more enhanced many-body interactions in 1D structures. The larger red shift can also be a result of the higher carrier densities (a few 10^{13} cm^{-2}) in our experiment than that previously reported in GaAs quantum wells (~10^{11}–10^{12} cm^{-2}).[23,67] In addition, there isn't a significant change of the periods for the energy shifts to red before and after AlGaAs-coating, consistent with the above dynamical analysis of carrier thermalization. Moreover, the initial rapid red-shift can still be observed in GaAs/AlGaAs upon 650 nm pump, even though the rapid decay is not obvious in this case. This might be additional evidence that the rapid decay immediately after the pump excitation is really buried by the rise process due to the charge transfer from AlGaAs to GaAs, as mentioned before.

In Stage II as carriers continue to cool down, BF and BGR can take effects simultaneously. In the BF process, the carriers occupy the available states from the bottom of the bands, resulting in the bleaching of the band-edge absorption, and thus manifests itself as an apparent blue-shift of E_g.[18] In contrast to BF, the BGR originates from screening of Coulomb repulsion among carriers, leading to a red-shift of E_g.[18] As shown in Fig. 4d and e, the $M_1(t)$ behavior of bare GaAs is similar to that of the GaAs/AlGaAs SNW-array when excited by an 800 nm laser. After the initial rapid red-shift, both of them involve a blue shift followed by a red shift before 5 ps, and then by a long-lived and slow blue-shift in Stage III, as will be discussed below. Except the final long-lived process, the blue and red shift crossover occur generally in the period of τ_2 (~5 ps) due to carrier cooling and transport processes. In this period, the carrier temperature is still much higher than the lattice and there is a strong competition between BF and BGR. These two effects can partially cancel each other and give rise to either a red or a blue-shift of the exciton resonance. A similar crossover phenomenon has been observed in optically excited 2D WS_2.[66] In addition, carrier transfer between different GaAs crystal phases, WZ and ZB, along the SNWs could also affect the evolution of carrier population and thus modulates the evolution of E_g.

In Stage III after 5 ps, the dynamics behaves as a slow blue-shift process, which can last tens or even hundreds of picoseconds before it recovers to its final equilibrium position. The time scale is compatible with the thermal dissipation time (τ_2) to the surroundings.[18] It is hardly satisfactory if we attribute the continuous blue-shift to BF, since the BF should be finished in the previous carrier cooling process.[18] A likely explanation is that after Stage II, the lattice temperature is heated by the hot carriers. After that, during the transfer of thermal energy from optical phonon to acoustic phonons in Stage III, the sample temperature at the probe focus slowly decreases, leading to the gradual expansion of the bandgap. The effect of bandgap expansion on exciton resonance is greater than that of the decrease of carrier distribution in this stage. The gradual blue-shift of the PL spectra in temperature-dependent measurement indeed demonstrates that E_g increases as the sample temperature cools down (see Fig. S4, ESI†). Finally, the blue and red-shift crossover in Stage II disappears upon 650 nm pump, and is replaced by a steady and slow blue-shift following Stage I, as shown in Fig. 4c. It is speculated here that it might be because the excitation energy at 650 nm is much higher than that at the probe wavelength. After the hot carriers relax to the band bottom, the carrier density and their temperatures are not as high as that with 800 nm excitation, so that the competition between BGR and BF is not strong enough to be illustrated in the moment trace.

Conclusions

In summary, the ultrafast carrier dynamics of GaAs and GaAs/AlGaAs SNW-arrays were investigated by transient absorption measurement. The transparent PDMS film containing an SNW-array was prepared by a simple spin coating and peeling off method. Conspicuous GSB signals due to the band-gap excitonic transition of GaAs were observed under 800 nm and 650 nm pumps. The GSB dynamics in GaAs and GaAs/AlGaAs SNW-arrays were compared. Three dynamics processes, including carrier thermalization, carrier cooling and thermal dissipation, were detected in GSB time traces under 800 nm pumps. The time constant of the carrier thermalization was firstly verified to be sub-0.5 ps, and it was found that the thermalization time is almost independent of the AlGaAs-coating. Except for the dynamics above, a rise process probably due to the charge transfer from the AlGaAs-shell to GaAs-core was observed with 650 nm excitation. The evolution of the band-gap energy of GaAs indicates that there is an initial rapid red-shift in the thermalization process, followed by a slow blue and red shift crossover before 5 ps, and then by an even slower blue shift. The slow blue and red shift crossover within 5 ps is probably due to the competition between BF and BGR, while the final slow blue-shift might originate from the decrease of the sample temperature in the thermal dissipation process. The results shed new lights on the basic physics of carrier scattering in the SNW-array and also are significant for the development of new flexible optoelectronic devices.

Conflicts of interest

There are no conflicts to declare.

Acknowledgements

This work is financially supported by the National Natural Science Foundation of China (grant no. 11774071, 61674021, 11674038, 61704011, 61904017, 11874125, 11704079), the Science and Technology Program of Guangzhou (grant no. 201904010104 and 201804010451), the State Key Laboratory of Luminescence and Applications (grant no. SKLA-2019-08), the Research and Development Project in a Key Area of Guangdong Province (grant no. 2020B090922001), and the Foundation of State Key Laboratory of High Power Semiconductor Lasers and the Project of Education Department of Jilin Province (JJKH20200763KJ).

Notes and references

1 G. Digeronimo, M. Petruzzella, S. Birindelli, R. Gaudio, S. Fattah Poor, F. van Otten and A. Fiore, *Photonics*, 2016, **3**, 55.
2 N. Guan, X. Dai, A. V. Babichev, F. H. Julien and M. Tchernycheva, *Chem. Sci.*, 2017, **8**, 7904–7911.
3 J. Valente, T. Godde, Y. Zhang, D. J. Mowbray and H. Liu, *Nano Lett.*, 2018, **18**, 4206–4213.
4 T. Zhai, L. Li, X. Wang, X. Fang, Y. Bando and D. Golberg, *Adv. Funct. Mater.*, 2010, **20**, 4233–4248.
5 D. Saxena, S. Mokkapati, P. Parkinson, N. Jiang, Q. Gao, H. H. Tan and C. Jagadish, *Nat. Photonics*, 2013, **7**, 963–968.
6 K. Peng, P. Parkinson, L. Fu, Q. Gao, N. Jiang, Y. N. Guo, F. Wang, H. J. Joyce, J. L. Boland, H. H. Tan, C. Jagadish and M. B. Johnston, *Nano Lett.*, 2015, **15**, 206–210.
7 X. Dai, S. Zhang, Z. Wang, G. Adamo, H. Liu, Y. Huang, C. Couteau and C. Soci, *Nano Lett.*, 2014, **14**, 2688–2693.
8 N. P. Dasgupta, J. Sun, C. Liu, S. Brittman, S. C. Andrews, J. Lim, H. Gao, R. Yan and P. Yang, *Adv. Mater.*, 2014, **26**, 2137–2184.
9 R. Yan, D. Gargas and P. Yang, *Nat. Photonics*, 2009, **3**, 569–576.
10 Y. Xia, P. Yang, Y. Sun, Y. Wu, B. Mayers, B. Gates, Y. Yin, F. Kim and H. Yan, *Adv. Mater.*, 2003, **15**, 353–389.
11 J. A. Czaban, D. A. Thompson and R. R. LaPierre, *Nano Lett.*, 2009, **9**, 148–154.
12 L. Ma, W. Hu, Q. Zhang, P. Ren, X. Zhuang, H. Zhou, J. Xu, H. Li, Z. Shan, X. Wang, L. Liao, H. Q. Xu and A. Pan, *Nano Lett.*, 2014, **14**, 694–698.
13 C. Zhou, X. T. Zhang, K. Zheng, P. P. Chen, W. Lu and J. Zou, *Nano Lett.*, 2017, **17**, 7824–7830.
14 S. A. Baig, J. L. Boland, D. A. Damry, H. H. Tan, C. Jagadish, H. J. Joyce and M. B. Johnston, *Nano Lett.*, 2017, **17**, 2603–2610.
15 J. P. Sprengers, A. Gaggero, D. Sahin, S. Jahanmirinejad, G. Frucci, F. Mattioli, R. Leoni, J. Beetz, M. Lermer, M. Kamp, S. Höfling, R. Sanjines and A. Fiore, *Appl. Phys. Lett.*, 2011, **99**, 181110.
16 E. M. Gallo, G. Chen, M. Currie, T. McGuckin, P. Prete, N. Lovergine, B. Nabet and J. E. Spanier, *Appl. Phys. Lett.*, 2011, **98**, 241113.
17 M. H. Huang, S. Mao, H. Feick, H. Yan, Y. Wu, H. Kind, E. Weber, R. Russo and P. Yang, *Science*, 2001, **292**, 1897–1899.
18 J. Shah, *Ultrafast Spectroscopy of Semiconductors and Semiconductor Nanostructures*, Springer, Berlin, Heidelberg, 1996.
19 R. P. Prasankumar, P. C. Upadhya and A. J. Taylor, *Phys. Status Solidi B*, 2009, **246**, 1973–1995.
20 S. O. Mariager, D. Khakhulin, H. T. Lemke, K. S. Kjaer, L. Guerin, L. Nuccio, C. B. Sorensen, M. M. Nielsen and R. Feidenhansl, *Nano Lett.*, 2010, **10**, 2461–2465.
21 R. Roder, T. P. H. Sidiropoulos, C. Tessarek, S. Christiansen, R. F. Oulton and C. Ronning, *Nano Lett.*, 2015, **15**, 4637–4643.
22 C. V. Shank, R. L. Fork, R. F. Leheny and J. Shah, *Phys. Rev. Lett.*, 1979, **42**, 112–115.
23 D. R. Wake, H. W. Yoon, J. P. Wolfe and H. Morkoc, *Phys. Rev. B: Condens. Matter Mater. Phys.*, 1992, **46**, 13452–13460.
24 M. Montazeri, H. E. Jackson, L. M. Smith, J. M. Yarrison-Rice, J. H. Kang, Q. Gao, H. H. Tan and C. Jagadish, *Nano Lett.*, 2012, **12**, 5389–5395.
25 M. A. Seo, S. A. Dayeh, P. C. Upadhya, J. A. Martinez, B. S. Swartzentruber, S. T. Picraux, A. J. Taylor and R. P. Prasankumar, *Appl. Phys. Lett.*, 2012, **100**, 071104.

26 D. Hulin, A. Mysyrowicz, A. Antonetti, A. Migus, W. T. Masselink, H. Morkoc, H. M. Gibbs and N. N. Peyghambarian, *Phys. Rev. B: Condens. Matter Mater. Phys.*, 1986, **33**, 4389–4391.
27 K. H. Schlaad, C. Weber, J. E. Cunningham, C. Hoof, G. Borghs, G. Weimann, W. Schlapp, H. Nickel and C. Klingshirn, *Phys. Rev. B: Condens. Matter Mater. Phys.*, 1991, **43**, 4268–4275.
28 P. Mante, S. Lehmann, N. Anttu, K. A. Dick and A. Yartsev, *Nano Lett.*, 2016, **16**, 4792–4798.
29 M. Mikulics, J. Zhang, J. Serafini, R. Adam, D. Grützmacher and R. Sobolewski, *Appl. Phys. Lett.*, 2012, **101**, 031111.
30 N. Jiang, Q. Gao, P. Parkinson, J. Wong-Leung, S. Mokkapati, S. Breuer, H. H. Tan, C. L. Zheng, J. Etheridge and C. Jagadish, *Nano Lett.*, 2013, **13**, 5135–5140.
31 C. Zhou, X. T. Zhang, K. Zheng, P. P. Chen, S. Matsumura, W. Lu and J. Zou, *Nanoscale*, 2019, **11**, 6859–6865.
32 N. Erhard, S. Zenger, S. Morkotter, D. Rudolph, M. Weiss, H. J. Krenner, H. Karl, G. Abstreiter, J. J. Finley and G. Koblmuller, *Nano Lett.*, 2015, **15**, 6869–6874.
33 P. Parkinson, J. Lloyd-Hughes, Q. Gao, H. H. Tan, C. Jagadish, M. B. Johnston and L. M. Herz, *Nano Lett.*, 2007, **7**, 2162–2165.
34 P. Parkinson, H. J. Joyce, Q. Gao, H. H. Tan, X. Zhang, J. Zou, C. Jagadish, L. M. Herz and M. B. Johnston, *Nano Lett.*, 2009, **9**, 3349–3353.
35 J. Giblin, F. Vietmeyer, M. P. McDonald and M. Kuno, *Nano Lett.*, 2011, **11**, 3307–3311.
36 M. A. Seyedi, M. Yao, J. D. Obrien, S. Y. Wang and P. D. Dapkus, *Appl. Phys. Lett.*, 2013, **103**, 251109.
37 L. Luo, J. Chen, M. Wang, H. Hu, C. Wu, Q. Li, L. Wang, J. Huang and F. Liang, *Adv. Funct. Mater.*, 2014, **24**, 2794–2800.
38 M. A. Seyedi, M. Yao, J. D. Obrien, S. Y. Wang and P. D. Dapkus, *Appl. Phys. Lett.*, 2014, **105**, 041105.
39 F. Li, Z. Li, L. Tan, Y. Zhou, J. Ma, M. Lysevych, L. Fu, H. H. Tan and C. Jagadish, *Nanotechnology*, 2017, **28**, 125702.
40 T. Frost, S. Jahangir, E. Stark, S. Deshpande, A. Hazari, C. Zhao, B. S. Ooi and P. Bhattacharya, *Nano Lett.*, 2014, **14**, 4535–4541.
41 Y. Lu and A. Lal, *Nano Lett.*, 2010, **10**, 4651–4656.
42 M. Yu, Y.-Z. Long, B. Sun and Z. Fan, *Nanoscale*, 2012, **4**, 2783.
43 G. Mariani, A. C. Scofield, C.-H. Hung and D. L. Huffaker, *Nat. Commun.*, 2013, **4**, 1497.
44 M. Yao, N. Huang, S. Cong, C.-Y. Chi, M. A. Seyedi, Y.-T. Lin, Y. Cao, M. L. Povinelli, P. D. Dapkus and C. Zhou, *Nano Lett.*, 2014, **14**, 3293–3303.
45 X. Y. Li, H. Guo, Z. Yin, T. Shi, L. Wen, Z. Zhao, M. Liu, W. Ma and Y. Wang, *J. Cryst. Growth*, 2011, **324**, 82–87.
46 X. Chen, N. Xia, Z. Yang, F. Gong, Z. Wei, D. Wang, J. Tang, X. Fang, D. Fang and L. Liao, *Nanotechnology*, 2018, **29**, 095201.
47 Z. Nie, R. Long, L. Sun, C. C. Huang, J. Zhang, Q. Xiong, D. W. Hewak, Z. Shen, O. V. Prezhdo and Z. H. Loh, *ACS Nano*, 2014, **8**, 10931–10940.
48 Z. Nie, R. Long, J. S. Teguh, C.-C. Huang, D. W. Hewak, E. K. L. Yeow, Z. Shen, O. V. Prezhdo and Z.-H. Loh, *J. Phys. Chem. C*, 2015, **119**, 20698–20708.
49 I. Vurgaftman, J. R. Meyer and L. R. Rammohan, *J. Appl. Phys.*, 2001, **89**, 5815–5875.
50 N. Peyghambarian, S. W. Koch and A. Mysyrowicz, *Introduction to semiconductor optics*, Prentice Hall, Division of Simon and Schuster One Lake Street Upper Saddle River, NJ, United States, 1993.
51 L. Ahtapodov, J. Todorovic, P. Olk, T. Mjaland, P. Slattnes, D. L. Dheeraj, A. T. J. Van Helvoort, B. O. Fimland and H. Weman, *Nano Lett.*, 2012, **12**, 6090–6095.
52 U. Jahn, J. Lahnemann, C. Pfuller, O. Brandt, S. Breuer, B. Jenichen, M. Ramsteiner, L. Geelhaar and H. Riechert, *Phys. Rev. B: Condens. Matter Mater. Phys.*, 2012, **85**, 045323.
53 A. De and C. E. Pryor, *Phys. Rev. B: Condens. Matter Mater. Phys.*, 2010, **81**, 155210.
54 B. Ketterer, M. Heiss, M. J. Livrozet, A. Rudolph, E. Reiger and A. F. I. Morral, *Phys. Rev. B: Condens. Matter Mater. Phys.*, 2011, **83**, 125307.
55 B. Ketterer, M. Heiss, E. Uccelli, J. Arbiol and A. F. I. Morral, *ACS Nano*, 2011, **5**, 7585–7592.
56 A. Senichev, P. Corfdir, O. Brandt, M. Ramsteiner, S. Breuer, J. Schilling, L. Geelhaar and P. Werner, *Nano Res.*, 2018, **11**, 4708–4721.
57 S. Schmittrink, D. S. Chemla and D. A. B. Miller, *Phys. Rev. B: Condens. Matter Mater. Phys.*, 1985, **32**, 6601–6609.
58 F. Ceballos, Q. Cui, M. Z. Bellus and H. Zhao, *Nanoscale*, 2016, **8**, 11681.
59 M. S. Brown and C. B. Arnold, Laser Precision Microfabrication, in *Fundamentals of Laser-Material Interaction and Application to Multiscale Surface Modification*, ed. K. Sugioka, M. Meunier and A. Piqué, Springer Berlin Heidelberg, Berlin, Heidelberg, 2010.
60 J. L. Boland, S. Conesa-Boj, P. Parkinson, G. Tütüncüoglu and M. B. Johnston, *Nano Lett.*, 2015, **15**, 1336–1342.
61 M. Montazeri, H. E. Jackson, L. M. Smith, J. M. Yarrison-Rice, J. H. Kang, Q. Gao, H. H. Tan and C. Jagadish, *Nano Lett.*, 2012, **12**, 5389–5395.
62 N. N. Peyghambarian, H. M. Gibbs, J. L. Jewell, A. Antonetti, A. Migus, D. Hulin and A. Mysyrowicz, *Phys. Rev. Lett.*, 1984, **53**, 2433–2436.
63 W. T. Pollard, S. Lee and R. A. Mathies, *J. Chem. Phys.*, 1990, **92**, 4012–4029.
64 C. Ruppert, A. Chernikov, H. M. Hill, A. F. Rigosi and T. F. Heinz, *Nano Lett.*, 2017, **17**, 644–651.
65 D. R. Wake, H. W. Yoon, J. P. Wolfe and H. Morko, *Phys. Rev. B: Condens. Matter Mater. Phys.*, 1992, **46**, 13452.
66 E. J. Sie, A. Steinhoff, C. Gies, C. H. Lui, Q. Ma, M. Rosner, G. Schonhoff, F. Jahnke, T. O. Wehling and Y. Lee, *Nano Lett.*, 2017, **17**, 4210–4216.
67 M. J. Rosker, F. W. Wise and C. L. Tang, *Appl. Phys. Lett.*, 1986, **49**, 1726–1728.

